



Cite this: *Soft Matter*, 2025,  
21, 2355

## Micropores can enhance the intrinsic fracture energy of hydrogels†

Puyu Cao, <sup>a</sup> Bin Chen, <sup>\*ab</sup> Yi Cao <sup>cd</sup> and Huajian Gao <sup>e</sup>

Hydrogels, a class of soft materials composed of a polymer chain network, are widely known to be prone to fatigue failure. To understand the underlying mechanisms, we simulate polymer scission and fatigue initiation in the vicinity of a crack tip within a two-dimensional polymer network. For a network without pores, our findings reveal that polymer scission can occur across multiple layers of chains, rather than just a single layer as assumed in the classical Lake–Thomas theory, consistent with previous studies. In contrast, for a network with a high density of micropores, our results demonstrate that the pores can substantially enhance the intrinsic fracture energy of the network in direct proportion to the pore size. This enhancement is attributed to pore–pore interactions, which lead to a relatively uniform distribution of cohesive energy ahead of the crack tip. Our model suggests that incorporating micro-pores could be a promising strategy for improving the intrinsic fracture energy of hydrogels and that natural porous tissues may have evolved to achieve enhanced fatigue resistance.

Received 13th August 2024,  
Accepted 20th February 2025

DOI: 10.1039/d4sm00973h

[rsc.li/soft-matter-journal](http://rsc.li/soft-matter-journal)

## Introduction

In recent years, synthetic hydrogels have undergone significant advancements and are increasingly utilized across various fields such as tissue engineering, agriculture, drug delivery, soft robotics, and flexible devices, among others.<sup>1–4</sup> Many of these applications require hydrogels to withstand cyclic loads, including repetitive loading on hydrogel-based biomimetic skins<sup>5</sup> and cartilage,<sup>6</sup> even though hydrogels are known to be susceptible to fatigue failure.<sup>7</sup> To tackle this challenge, a number of hydrogels with elevated fatigue thresholds have been developed using various strategies.<sup>8–10</sup>

The fatigue threshold of hydrogels is primarily attributed to their intrinsic fracture energy,<sup>11,12</sup> which corresponds to the limit below which fatigue cracks do not propagate. Generally, viscosity or dynamics are not considered when calculating such a limit. The fatigue threshold has traditionally been evaluated<sup>11,13–17</sup> using the Lake–Thomas theory,<sup>18</sup> which focuses on the breakage

of a single layer of polymer chains across the crack plane (Fig. 1a) without triggering inelastic deformation in the bulk. The thickness of a chain layer in its unstrained state can be approximated, for instance, by the equilibrium separation between two ends of an individual polymer chain in the freely-jointed chain model. Theoretical predictions have demonstrated good agreement with experimental findings across various polymeric materials, such as PAAm–Ca–alginate,<sup>19,20</sup> PAAm–PAMPS,<sup>13</sup> and PAAm–polyvinyl alcohol.<sup>11</sup> Nevertheless, a source of uncertainty arises from estimating the thickness of the energy-dissipating layer, and open questions remain regarding why chain scission appears confined to a single layer rather than involving multiple layers of chains.<sup>19</sup>

High-density pores are often introduced in hydrogels through phase separation during synthesis.<sup>21</sup> SEM images of polyacrylamide hydrogels reveal a multitude of micropores with diameters of approximately 2 µm (Fig. 1b), through which microbeads can diffuse (Fig. 1c). The average pore size,<sup>22</sup> pore size distribution, and interconnections between pores are crucial aspects of a hydrogel matrix. Notably, in freeze-dried hydrogels derived from silk fibroin solutions, pore sizes diminish with increasing silk fibroin concentration and decrease with rising temperature at a constant silk fibroin concentration.<sup>23</sup> Hydrogels freeze-dried with Ca<sup>2+</sup> exhibit larger pore sizes compared to those without Ca<sup>2+</sup> ions in the silk fibroin aqueous solutions.<sup>24</sup> Various technologies, including solvent casting particle leaching,<sup>25</sup> freeze-drying,<sup>26</sup> gas foaming,<sup>27</sup> and electrospinning,<sup>28</sup> have been deployed to regulate the microarchitectural features of pores in hydrogels and facilitate the creation of functional hydrogels that mimic native tissue structures, thereby enhancing cell viability,<sup>29</sup> proliferation<sup>30</sup> and migration.<sup>31</sup>

<sup>a</sup> Department of Engineering Mechanics, Zhejiang University, Hangzhou, People's Republic of China. E-mail: chenb6@zju.edu.cn

<sup>b</sup> Key Laboratory of Soft Machines and Smart Devices of Zhejiang Province, Hangzhou, People's Republic of China

<sup>c</sup> School of Physics, Nanjing University, Nanjing, China

<sup>d</sup> Collaborative Innovation Center of Atmospheric Environment and Equipment Technology, Jiangsu Key Laboratory of Atmospheric Environment Monitoring and Pollution Control, School of Environmental Science and Engineering, Nanjing University of Information Science & Technology, Nanjing 210044, P. R. China

<sup>e</sup> Mechano-X Institute, Applied Mechanics Laboratory, Department of Engineering Mechanics, Tsinghua University, Beijing 100084, China

† Electronic supplementary information (ESI) available. See DOI: <https://doi.org/10.1039/d4sm00973h>



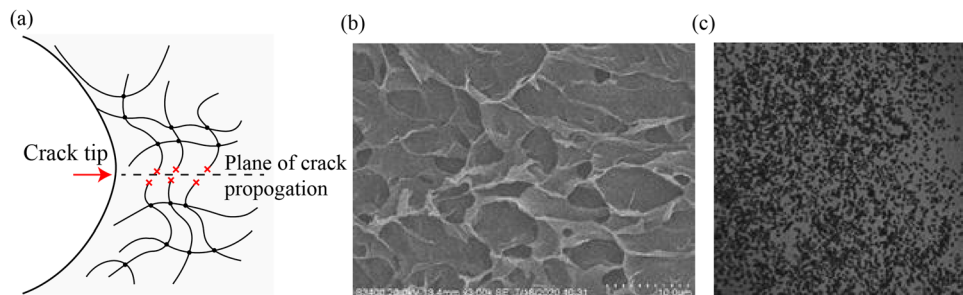


**Fig. 1** Classical Lake–Thomas theory and evidence for the existence of micropores in hydrogels. (a) A schematic illustration of the Lake–Thomas theory, which assumes that the intrinsic fracture energy of a polymer is due to the scission of a layer of polymer chains along the prospective crack plane. (b) An SEM image of polyacrylamide hydrogel showing small pores with diameters of approximately 2  $\mu\text{m}$ . (c) Verification of pore size through the free diffusion of beads with diameters of approximately 2  $\mu\text{m}$ .

This study aims to investigate the effect of micropores on the intrinsic fracture energy of the polymer network in a hydrogel. We begin by validating the Lake–Thomas theory<sup>18</sup> using a two-dimensional (2D) chain network model with a pre-existing crack. Our results from the polymer network model indicate that multiple layers of chains are involved in crack advance at the fatigue threshold, thereby challenging the assumption in the Lake–Thomas theory. Nevertheless, our simulation results are in agreement with the commonly held view in the literature that the intrinsic fracture energy of a polymer network generally scales with and is thus limited by the initial length of individual chains. To determine whether it is possible to overcome this size limitation imposed by the initial chain length, we subsequently simulate the polymer chain scission and fatigue initiation in the vicinity of a crack in a 2D soft material containing a high density of micropores by integrating the finite element method (FEM) and the polymer network model at the crack tip. Our findings reveal that the presence of pores alters the stress distribution within the material, leading to a significant enhancement of the intrinsic fracture energy, which can scale with and be substantially enhanced by the pore size under certain conditions. Our study provides an integrated modeling framework for understanding the intrinsic fracture energy of both non-porous and porous hydrogels, with results highlighting the potential for designing hydrogels with specific microarchitectural features to improve the intrinsic fracture energy.

## Validation of the Lake–Thomas theory

Several polymer chain network models were recently developed<sup>32–35</sup> to investigate the mechanical behaviors of polymeric materials. To validate the classical Lake–Thomas theory, we constructed a 2D polymer chain network in COMSOL, which is convenient to use and differs from most of the previous polymer chain network models. Our chain network is composed of truss elements representing individual polymer chains, as well as solid elements for sustaining 2D hydrostatic pressure. Within the network, polymer chains are periodically distributed and form triangular meshes. Prestress is introduced into the network (e.g., due to water swelling) such that each polymer chain of initial length  $l_0$  displays the same end-to-end distance of  $l_d$ .

Individual nodes of truss elements physically correspond to crosslinks in the chain network. The worm-like chain model<sup>36</sup> is chosen to describe the force–stretch behavior of each individual polymer chain,  $F = \frac{kT}{P} \left( \frac{1}{4} \left( 1 - \frac{x}{L_c} \right)^{-2} - \frac{1}{4} + \frac{x}{L_c} \right)$ , where  $k$  is Boltzmann's constant,  $T$  the temperature,  $P$  the persistence length,  $L_c$  the contour length, and  $x$  the end-to-end distance of the polymer chain. 2D solid elements are adopted to maintain the in-plane near incompressibility of a neo-Hookean hyperelastic material, with a sufficiently large bulk modulus  $\kappa$  and a small shear modulus  $G$ , ensuring an approximately equibiaxial (2D hydrostatic) stress state (Tables 1–3).

To use the polymer chain network model to simulate the intrinsic fracture energy, we consider a 2D strip with a crack under uniaxial loading, as illustrated in Fig. 2a. In the simulation, only half of the polymer chain network is modeled, with symmetry boundary conditions applied at the bottom edge along the crack propagation path and at the left edge, which is sufficiently far from the crack tip to ensure good convergence.

Typical force contours and deformation pattern from the simulation are displayed in Fig. 2b. The simulation terminates when the force of any individual chain reaches a predefined critical value  $F_c$ , referred to as the chain breaking force. The intrinsic fracture energy of the network is then evaluated through the J-integral,<sup>37</sup>

$$J = \varepsilon_0 h \quad (1)$$

where  $\varepsilon_0$  is the strain energy density far ahead of the crack tip and  $h$  the height of the strip. As displayed in Fig. 2c, the simulated intrinsic fracture energy increases with  $F_c$ .

According to the Lake–Thomas theory,<sup>18</sup> the intrinsic fracture energy  $\Gamma_0$  could be expressed as  $\Gamma_0 \simeq w_0 \bar{L}$ , where  $\bar{L}$  is the initial chain length typically  $\sim 10$  nm, and  $w_0$  the critical strain energy density for chain rupture at the crack tip. Following the force–stretch curve of a worm-like chain,  $w_0$  can be calculated

**Table 1** Default parameters used in the worm-like chain model

$l_d$	$P$	$L_c$	$kT$	$G$	$\kappa$
24 nm	0.4 nm	80 nm	4.14 pN nm	$10^{-5}$ pN nm $^{-2}$	10 pN nm $^{-2}$



Table 2 Default parameters for the Langevin chain model in the polymer chain network

$l_d$	$P$	$L_c$	$l_0$	$kT$	$G$	$\kappa$
24 nm	0.4 nm	80 nm	8 nm	4.14 pN nm	$10^{-3}$ pN nm $^{-2}$	$100$ pN nm $^{-2}$

Table 3 Default model parameters for porous hydrogels used in the simulation

$\mu$	$\lambda_m$	$a$	$t$	$F_c$
0.005 MPa	1.2	2 $\mu$ m	0.5 $\mu$ m	500 pN

for given  $F_c$ , and the prediction according to the Lake–Thomas theory is plotted in Fig. 2c and d.

As shown in Fig. 2c and d, our results agree well with the prediction by the Lake–Thomas theory at relatively low  $F_c$  or  $w_0$ , where the corresponding bond breaking force falls below  $\sim 100$  pN. At relatively high  $F_c$  or  $w_0$ , e.g., as the bond breaking force reaches  $\sim 1$  nN, our simulated intrinsic fracture energy is significantly larger than the prediction of the Lake–Thomas theory, with up to  $\sim 500\%$  discrepancy. It should be noted that we have adopted a modern description of the Lake–Thomas theory<sup>18</sup> in the current work, where the energy for the rupture of a single polymer chain is calculated as the integral of the force–stretch curve of the worm-like chain.<sup>36</sup> In our view, this approach is more reasonable than the original treatment

proposed in the Lake–Thomas theory,<sup>18</sup> which assumes that the energy required to rupture a single polymer chain is the product of the number of chemical bonds in the main chain and the rupture energy of a single chemical bond. However, we acknowledge that the discrepancy between the theory and simulation, as shown in Fig. 2, could be smaller if the original treatment from the Lake–Thomas theory<sup>18</sup> were adopted.

To understand the origin of such discrepancy, we plot the force contour of individual chains in the vicinity of the crack tip. As shown in Fig. 3a–c, the chain forces are highly concentrated at the crack tip and decay rapidly over a few neighboring chains. The decay distance along the vertical direction increases with  $F_c$ . We let the crack tip advance by breaking a single polymer chain at the crack tip and calculate the associated changes in chain force within the network. The results in Fig. 3d–f reveal that the dissipation zone associated with crack propagation can involve a few layers in the vertical direction, and the larger the  $F_c$ , the more layers are involved.

The above results indicate that multiple layers of chains are involved in crack advance at the fatigue threshold, thereby challenging the assumption in the Lake–Thomas theory that

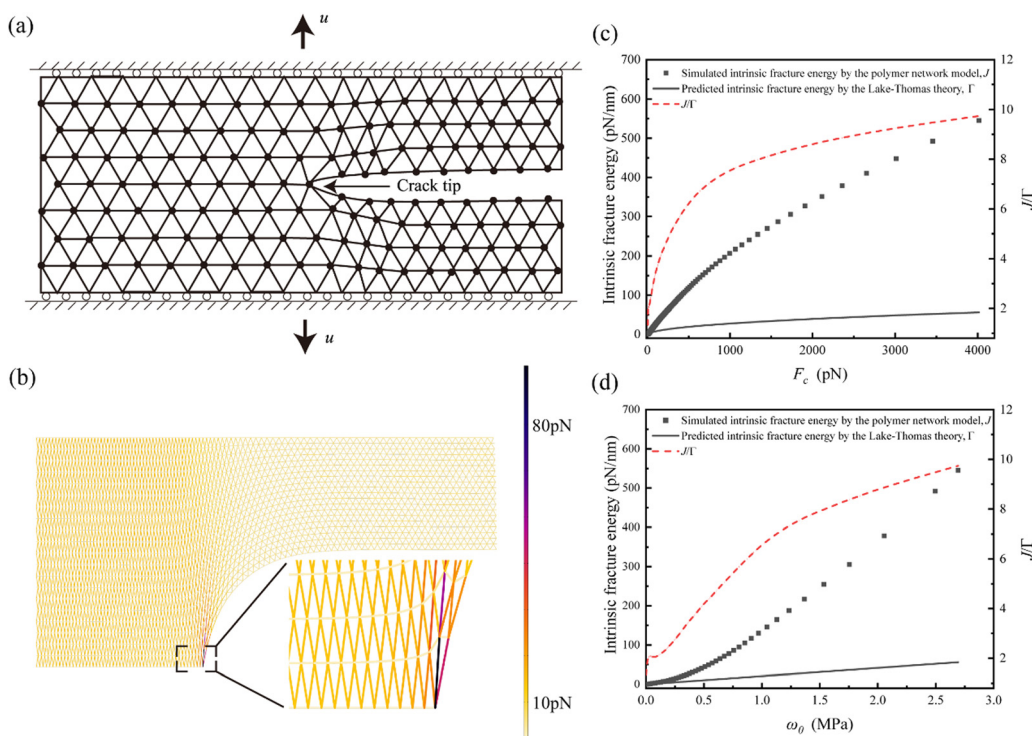


Fig. 2 Comparison between simulated intrinsic fracture energy and predictions from the Lake–Thomas theory. (a) Simulation of a crack propagating in a strip of a triangular polymer chain network. (b) Simulated chain force contours and deformed configuration. (c) Comparison between the simulated intrinsic fracture energy and predictions from the Lake–Thomas theory as a function of critical chain force. (d) Comparison between the simulated intrinsic fracture energy and predictions from the Lake–Thomas theory as a function of critical strain energy density.



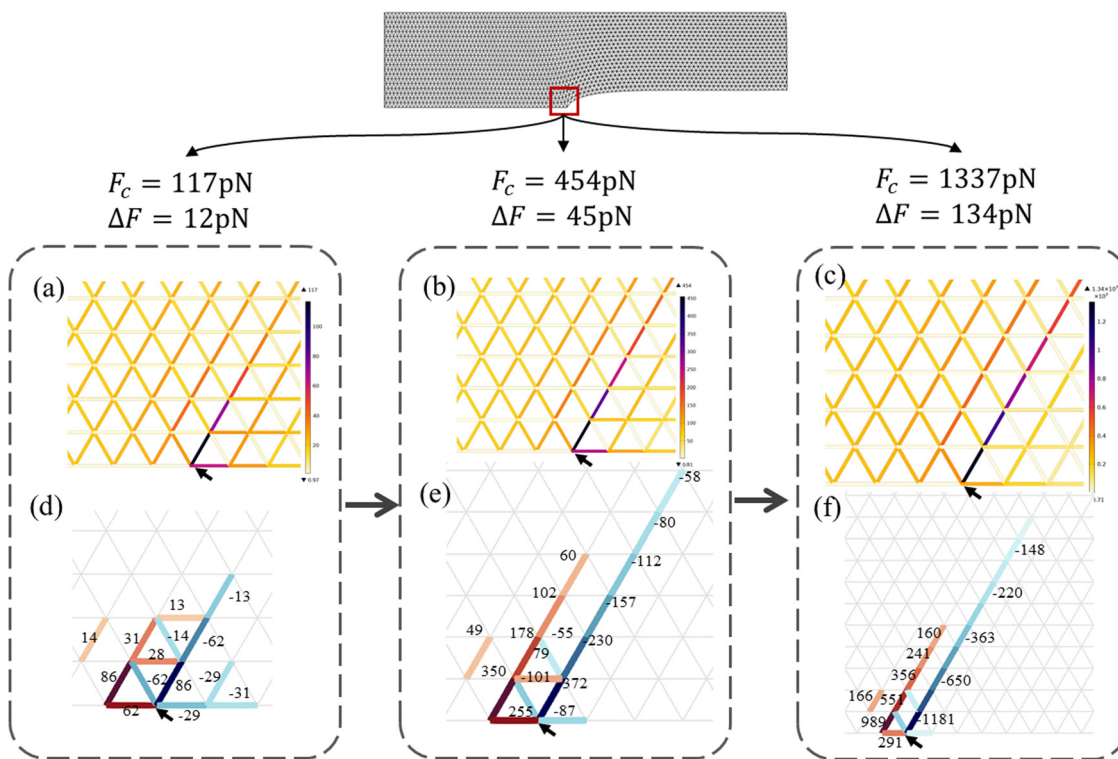


Fig. 3 Simulated crack tip force and deformation fields. (a)–(c) Chain force contours in the vicinity of the crack tip under different  $F_c$ . (d)–(f) Change in chain forces upon crack propagation by breaking a single polymer chain at the crack tip under different  $F_c$ . Only changes in chain force above a small threshold value,  $\Delta F$ , are plotted, where,  $\Delta F = 12$  pN in (d), 45 pN in (e), and 134 pN in (f), respectively.

only a single layer of polymer chains contributes to the intrinsic fracture energy of a polymeric material, especially when the chain-breaking force can reach that of a covalent bond on the order of approximately 1 nN.<sup>38</sup> Nevertheless, our simulation results are in agreement with the commonly held view in the literature<sup>7</sup> that the intrinsic fracture energy of a polymer network—following the worm-like chain theory<sup>36</sup> for the force–stretch behavior of individual chains and assuming a chain-breaking force below approximately 1 nN—generally scales with, and is therefore limited by, the initial length of individual chains, *i.e.*

$$J_0 \sim w_0 \bar{L} \quad (2)$$

## Result

To explore the possibility of overcoming the size limitation imposed by the initial chain length in eqn (2), we next investigate the intrinsic fracture energy of a polymer network with periodically distributed pores, where the polymer matrix forms a network-like structure at a much larger scale than a single polymer chain. Similar to experiments,<sup>39</sup> the pure-shear model of a plane-stress cracked strip is employed to determine the intrinsic fracture energy (Fig. 4a). In this model, pores with radius  $a$  are square-shaped with rounded corners and are uniformly distributed in two patterns: stacked and staggered, as illustrated in Fig. 4b and c. The walls between neighboring pores have a consistent thickness  $t$ . Since a soft or debonded

inclusion tends to attract cracks,<sup>40</sup> we focus on the scenario where the crack tip is situated within a pore.

Using a two-scale approach, we integrate the polymer network model with the traditional FEM to simulate a strip containing a high density of pores. First, we simulate the stretching of the porous structures at the macroscopic scale using FEM to obtain the global displacement field. Then, we focus on a region near the crack tip and build the corresponding polymer network model containing a few pores at the microscopic scale, as shown in Fig. 5e, h and Fig. S1, S2 (ESI<sup>†</sup>). Following some of the examples provided in COMSOL, the displacements along the interacting boundaries of the polymer network model with the macroscopic porous structure are directly obtained from the FEM simulation and fixed during the micro-scale polymer network simulation. This approach can be justified by recognizing that FEM analysis is expected to hold in regions relatively far from the crack tip, where stress variations are gradual, while the polymer network model offers refined analysis near the crack tip, where stress changes more rapidly. This step-by-step simulation process concludes when the maximum force within the chains in the polymer network model near the crack tip reaches the critical force value. At this point, the corresponding intrinsic fracture energy is calculated using the J-integral.<sup>37</sup> A flowchart of the simulation scheme described above is provided in Fig. S3 (ESI<sup>†</sup>).

This two-scale methodology begins with an initial simulation using the FEM in COMSOL. Taking advantage of symmetry, only half of the strip is modeled. The strip length is chosen to be



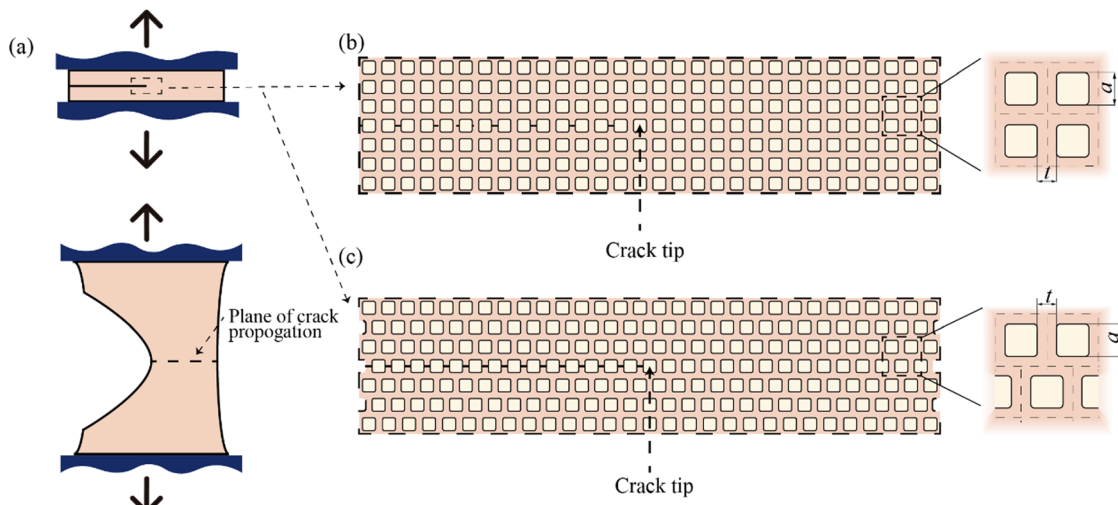


Fig. 4 Simulation model of a porous polymer network. (a) A mode I crack propagating in a hydrogel strip with pores. (b) Stacked pores. (c) Staggered pores.

sufficiently large, and the horizontal displacement is constrained at the far right side of the strip to enhance convergence. For simplicity and without loss of generality, in the FEM, we employ the incompressible Arruda-Boyce model,<sup>41</sup> which incorporates two material parameters: the locking stretch  $\lambda_m$  of polymer chains, and the shear modulus  $\mu$ .

At the lower scale, we focus on a localized region near the crack tip, where the displacements calculated from the FEM are imposed as boundary conditions to model the forces and stretches within the polymer chain network. For the truss elements, we employ the polynomial series of the Langevin chain model<sup>42-44</sup> to describe the force-stretch behavior of individual chains,

$$F = \frac{kT}{2P} \left( 3 \frac{x}{L_c} + \frac{9}{5} \left( \frac{x}{L_c} \right)^3 + \frac{297}{175} \left( \frac{x}{L_c} \right)^5 + \frac{1539}{875} \left( \frac{x}{L_c} \right)^7 + \frac{126117}{37375} \left( \frac{x}{L_c} \right)^9 \right).$$

In addition, solid elements are adopted to model a nearly incompressible neo-Hookean hyperelastic material with a large bulk modulus of  $\kappa$  and a small shear modulus of  $G$ . The hydrostatic stress in the solid elements is enforced as

$$F_3 / \left( \frac{\sqrt{3}}{2} l_d^2 \right),$$

where  $F_3$  is the Langevin chain force with extension  $\lambda_3 l_d$ ,  $\lambda_3$  being the out-of-plane stretch. Note that, in the employed Arruda-Boyce model,<sup>41</sup>  $\mu$  is obtained by fitting the stress-stretch curves under uniaxial tension and  $\lambda_m = \sqrt{L_c/2P}/\lambda_s$ ,  $\lambda_s$  denoting the free-swelling stretch.

The two-scale simulation continues until the maximum chain force in the vicinity of the crack tip reaches the critical threshold value,  $F_c$ . At this point, we evaluate the average strain energy  $w_1$  far ahead of the crack tip and determine the intrinsic fracture energy  $J$  as the product of  $w_1$  and the strip height<sup>37</sup> under two sets of parameters: the first set varies the pore size while keeping the wall thickness fixed, and the second set changes the wall thickness while maintaining a constant pore size. The computed  $J/w_0$  are displayed in Fig. 5. The simulation results shown in

Fig. 5 indicate that  $J/w_0$  can significantly exceed  $\bar{L}$  for both pore patterns. The simulated  $J$  increases almost linearly with pore size under fixed wall thickness (Fig. 5a). Conversely, enlarging the wall thickness under fixed constant pore size only affects  $J/w_0$  slightly (Fig. 5b). The effect of the chain breaking force,  $F_c$ , is displayed in Fig. 5c, where  $J/(w_0 a)$  increases with  $F_c$ .

To make sense of the simulation results, we examine the deformation and force distribution in the crack tip region. As shown in Fig. 5d-i for both stacked and staggered pore patterns, the walls directly at the crack tip are largely under uniaxial loading with a nearly uniform strain energy density distribution. This is mainly attributed to the pore-pore interaction. Without this interaction, chain forces within the walls near the crack tip would be highly concentrated, as predicted by classical fracture mechanics theories.<sup>45</sup> As shown in Fig. S4 (ESI†), the chain forces within the wall closest to the crack tip become more evenly distributed as the pore size increases.

To understand why the intrinsic fracture energy scales with pore size, we note that the walls between pores near the crack tip can be regarded as a type of supercohesive bonds, where the stored elastic energy is released upon crack propagation (Fig. 6). For an interface with a periodic cohesive energy distribution, it has been shown that the apparent fracture energy falls between the peak and average values of the cohesive energy, depending on the relationship between the size of the cohesive zone and the periodicity of the energy distribution,  $l_c$ , and the period of the cohesive energy distribution,  $l_p$ .<sup>46</sup> For  $l_c \ll l_p$ , the apparent fracture energy of the interface is the peak value of the cohesive energy. Conversely, when  $l_p \ll l_c$ , the apparent fracture energy of the interface becomes equal to the average value of the cohesive energy.

In the case of a highly porous hydrogel network displayed in Fig. 4, the average cohesive energy is

$$\gamma_{\text{aveg}} \sim \frac{w_0 \cdot t \cdot a}{a + t} \sim w_0 t, \quad (3)$$



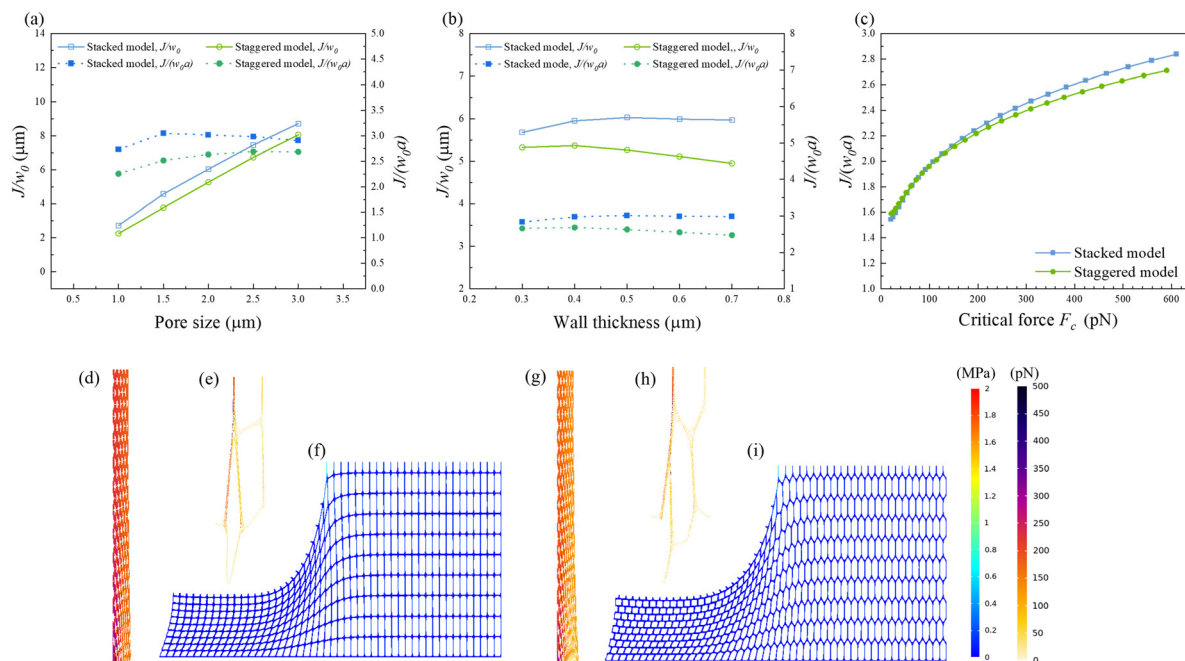


Fig. 5 Simulation results. (a) Simulated  $J/w_0$  is nearly proportional to the pore size under fixed wall thickness, and the nondimensional value  $J/w_0a \sim 2.5$  for all cases; (b) under fixed pore size,  $J/w_0$  varies little with the wall thickness and  $J/w_0a \sim 2.5$  for all cases; (c)  $J/w_0a$  increases with  $F_c$ ; typical simulated force contours within the walls at the crack tip in the stacked model (d) and (e) and in the staggered model (g) and (h); typical simulated strain energy density contours in the stacked model (f) and staggered model (i). Note that the strain energy density distribution is almost uniform at the crack tip.

which roughly scales with the wall thickness between neighboring pores, considering that  $a$  is generally larger than  $t$ . The peak value of the cohesive energy is

$$\gamma_{\text{peak}} \sim \frac{w_0 \cdot t \cdot a}{t} = w_0 a, \quad (4)$$

which scales with the pore size.

As shown in Fig. 5a and b, the simulated intrinsic fracture energy is roughly

$$J_1 \sim 2.5 w_0 a, \quad (5)$$

suggesting that the intrinsic fracture energy corresponds more closely to the peak value of cohesive energy as described in eqn (5) in our current analysis. This finding is consistent with the theory proposed by Chen *et al.*,<sup>46</sup> particularly when the cohesive zone size at the onset of fatigue is relatively small compared to the pore size. Furthermore, the numerical factor of 2.5 obtained from the simulation indicates that energy stored in multiple layers of walls significantly contributes to the intrinsic fracture energy.

## Discussion and conclusion

A chain network model has been developed to investigate the intrinsic fracture energy of hydrogels and to compare it with the Lake–Thomas theory, which relates intrinsic fracture energy to the breaking of a single layer of polymer chains along the crack plane. By employing force–stretch curves of individual chains based on the worm-like chain theory<sup>36</sup> and accounting for the impressibility of the network, our findings generally support a broad interpretation of the Lake–Thomas theory, demonstrating that the intrinsic fracture energy scales with the initial length of the constituent polymer chains and involves a chain-breaking force that is not excessively high. Our analysis reveals that chain scission is typically not confined to a single layer of chains but can involve multiple layers, as recently speculated in the literature.<sup>19</sup>

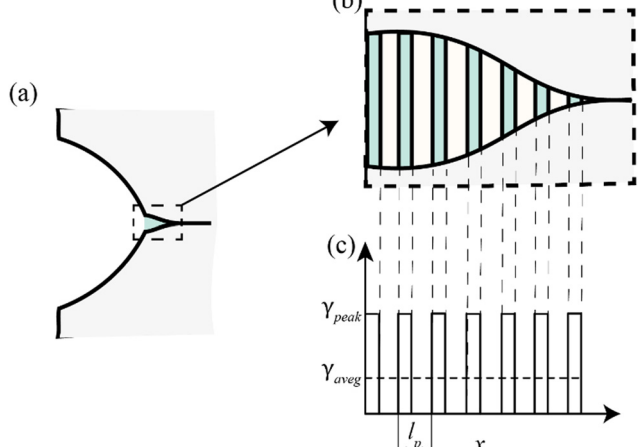


Fig. 6 Cohesive model of crack propagation in porous hydrogel networks. (a) Schematic of a cohesive crack model incorporating periodic supercohesive bonds. (b) Representation of the walls between pores in a porous hydrogel network as periodic supercohesive bonds. (c) Modeling of periodic cohesive bonds as a periodic distribution of cohesive energy.



It should be noted that in deriving the classical Lake–Thomas theory,<sup>18</sup> it was assumed that nearly all monomer units within a single polymer chain would rupture simultaneously during chain dissociation. However, this assumption does not necessarily hold true in reality. The more modern Lake–Thomas theory addresses this limitation by employing the critical strain energy density, calculated based on the integration of the force–extension curve of a single polymer chain upon dissociation. This modern formulation, as represented by eqn (2) in our work, is now widely used in predicting the fatigue threshold of soft materials.<sup>7,12,47</sup> Interestingly, a similar form of eqn (2) was also introduced in the original work by Lake and Thomas,<sup>18</sup> under the section titled Alternative Approach.

Our analysis is consistent with a recent study,<sup>48</sup> where energy dissipation from chains far from the crack tip was found to contribute to the intrinsic fracture energy of polymer networks. In that work,<sup>48</sup> the intrinsic fracture energy of polymer networks was also found to be several times the Lake–Thomas prediction when the ratio of the stiff energetic modulus to the soft entropic modulus of individual chains in their polymer network model was approximately 1000.<sup>48</sup> However, when this ratio increased to a very high value, for example,  $2 \times 10^4$ , along with the selection of a very high chain-breaking force of 5 nN, the intrinsic fracture energy was found to be almost two orders of magnitude higher than the Lake–Thomas prediction.<sup>48</sup> It is important to note that incompressibility was not enforced in their polymer network model,<sup>48</sup> despite it being a general requirement for soft polymeric materials. In contrast, incompressibility has been properly incorporated in our polymer network model.

Recently, through a combination of simulations and experiments, a new scaling law for the intrinsic fracture energy of polymer networks composed of stretchable strands was revealed.<sup>49</sup> This scaling law demonstrated its applicability across multiple length scales and indicated that the Lake–Thomas theory is not applicable, particularly when the force–stretch curve of a single strand in the network is highly nonlinear. In such cases, energy dissipation during crack propagation involves multiple layers of chains. Additionally, the scaling law suggested that the intrinsic fracture energy of a polymer network can be significantly enhanced by increasing the length of individual strands. These findings are consistent with our own results considering rather uniform stress distribution with individual strands.

In calculating the intrinsic fracture energy of a polymer network with periodically distributed pores using the integration of FEM and the chain network model, our analysis further indicates that the intrinsic fracture energy of a highly porous network can scale with the pore size rather than the chain length. Considering that chain lengths are typically on the order of approximately 10 nm and pore sizes on the order of approximately 1  $\mu\text{m}$ , this implies that the intrinsic fracture energy of a highly porous network could reach orders of magnitude higher than that of a homogeneous network. In other words, our analysis suggests that micropores in soft materials could significantly magnify the intrinsic fracture energy under certain conditions.

The intrinsic fracture energy of polymer networks, as measured in experiments,<sup>14,17,50</sup> was found to be nearly two orders

of magnitude greater than the Lake–Thomas prediction.<sup>48</sup> This substantial discrepancy was previously attributed to a nonlocal energy dissipation mechanism involving the relaxation of chains far from the crack tip, which is closely tied to the high ratio of the stiff energetic modulus to the soft entropic modulus of individual chains within the polymers.<sup>48</sup> However, based on eqn (2)–(4), our studies suggest an alternative explanation: the presence of micropores within polymers may contribute to this significant difference in intrinsic fracture energy.

In our simulations, the distribution of strain energy density across the wall thickness between neighboring pores is nearly uniform. However, this uniformity does not hold as the wall thickness becomes sufficiently large, which could reduce the amount of strain energy stored prior to reaching the fatigue threshold. Consequently, this leads to an intrinsic fracture energy that is lower than previously predicted. In this context, it is important to note that there exists a critical wall thickness for flaw tolerance, below which the strain energy density distribution remains uniform.<sup>51</sup> Therefore, introducing sufficiently small, densely packed, and hierarchically structured pores with appropriately thin walls could be an effective strategy to achieve a more uniform distribution of strain energy density and significantly enhance the intrinsic fracture energy.

Indeed, the fabrication of hydrogels with hierarchical pores is a promising area of research. For instance, the integration of directional freeze-casting and subsequent salting-out treatments has recently enabled the fabrication of hydrogels with multi-length-scale hierarchical structures.<sup>52</sup> These hydrogels feature micrometer-scale honeycomb-like pore walls composed of interconnected nanofibril meshes. Despite having a water content of up to 95 percent, these hydrogels exhibit high strength, toughness, and fatigue threshold, making them comparable to other robust hydrogels and even natural tendons.

Our analysis also suggests that the ubiquitous pores present in native tissues may play a role in contributing to their intrinsic fracture energy, potentially enhancing their resistance to cyclic loading. For instance, both experimental and simulation data have shown that the presence of pores in echinoderm stereom can reduce stress concentrations within the stereom, enabling high relative strength and significant energy absorption capabilities.<sup>53</sup> Similarly, diffused damage in bone, often caused by daily activities, typically spans approximately 1  $\mu\text{m}$  in length and has been shown to be highly effective in energy absorption.<sup>54</sup> Interestingly, our analysis suggests that age-related reductions in the formation of such diffused damage may partly account for the decline in fracture properties observed in aging bones.

## Data availability

The data that support the findings of this study are available from the corresponding author upon reasonable request.

## Conflicts of interest

There are no conflicts of interest to declare.



## Acknowledgements

This work was supported by Zhejiang Provincial Natural Science Foundation of China (Grant No.: LZ23A020004) and the National Natural Science Foundation of China (Grant No.: 12372318).

## References

- 1 M. Farokhi, F. Jonidi Shariatzadeh, A. Solouk and H. Mirzadeh, *Int. J. Polym. Mater.*, 2020, **69**, 230–247.
- 2 K. Y. Lee and D. J. Mooney, *Chem. Rev.*, 2001, **101**, 1869–1880.
- 3 Y. Lee, W. J. Song and J. Y. Sun, *Mater. Today Phys.*, 2020, **15**, 100258.
- 4 S. Lin, H. Yuk, T. Zhang, G. A. Parada, H. Koo, C. Yu and X. Zhao, *Adv. Mater.*, 2016, **28**, 4497–4505.
- 5 G. Su, J. Cao, X. Zhang, Y. Zhang, S. Yin, L. Jia, Q. Guo, X. Zhang, J. Zhang and T. Zhou, *J. Mater. Chem. A*, 2020, **8**, 2074–2082.
- 6 J. Liu, S. Lin, X. Liu, Z. Qin, Y. Yang, J. Zang and X. Zhao, *Nat. Commun.*, 2020, **11**, 1071.
- 7 J. Tang, J. Li, J. J. Vlassak and Z. Suo, *Extreme Mech. Lett.*, 2017, **10**, 24–31.
- 8 H. Lei, L. Dong, Y. Li, J. Zhang, H. Chen, J. Wu, Y. Zhang, Q. Fan, B. Xue, M. Qin, B. Chen, Y. Cao and W. Wang, *Nat. Commun.*, 2020, **11**, 4032.
- 9 S. Lin, X. Liu, J. Liu, H. Yuk, H. C. Loh, G. A. Parada, C. Settens, J. Song, A. Masic, G. H. McKinley and X. Zhao, *Sci. Adv.*, 2019, **5**, eaau8528.
- 10 C. Xiang, Z. Wang, C. Yang, X. Yao, Y. Wang and Z. Suo, *Mater. Today*, 2020, **34**, 7–16.
- 11 R. Bai, J. Yang, X. P. Morelle, C. Yang and Z. Suo, *ACS Macro Lett.*, 2018, **7**, 312–317.
- 12 X. Li and J. P. Gong, *Nat. Rev. Mater.*, 2024, **9**, 380–398.
- 13 W. Zhang, X. Liu, J. Wang, J. Tang, J. Hu, T. Lu and Z. Suo, *Eng. Fract. Mech.*, 2018, **187**, 74–93.
- 14 Y. Akagi, H. Sakurai, J. P. Gong, U. Chung and T. Sakai, *J. Chem. Phys.*, 2013, **139**, 144905.
- 15 C. Yang and Z. Suo, *Nat. Rev. Mater.*, 2018, **3**, 125–142.
- 16 K. Mayumi, C. Liu, Y. Yasuda and K. Ito, *Gels*, 2021, **7**, 91.
- 17 C. W. Barney, Z. Ye, I. Sacligil, K. R. McLeod, H. Zhang, G. N. Tew, R. A. Riggleman and A. J. Crosby, *Proc. Natl. Acad. Sci. U. S. A.*, 2022, **119**, e2112389119.
- 18 G. J. Lake and A. G. Thomas, *Proc. R. Soc. London, Ser. A*, 1967, **300**, 108–119.
- 19 R. Bai, J. Yang and Z. Suo, *Eur. J. Mech. – ASolids*, 2019, **74**, 337–370.
- 20 W. Zhang, J. Hu, J. Tang, Z. Wang, J. Wang, T. Lu and Z. Suo, *ACS Macro Lett.*, 2019, **8**, 17–23.
- 21 S. Wang, L. Li, D. Su, K. Robin and K. A. Brown, *ACS Appl. Mater. Interfaces*, 2018, **10**, 34604–34610.
- 22 S. M. Lanasa, I. T. Hoffecker and S. J. Bryant, *J. Biomed. Mater. Res., Part B*, 2011, **96**, 294–302.
- 23 M. Li, Z. Wu, C. Zhang, S. Lu, H. Yan, D. Huang and H. Ye, *J. Appl. Polym. Sci.*, 2001, **79**, 2192–2199.
- 24 U.-J. Kim, J. Park, C. Li, H.-J. Jin, R. Valluzzi and D. L. Kaplan, *Biomacromolecules*, 2004, **5**, 786–792.
- 25 R. V. Badhe, D. Bijukumar, D. R. Chejara, M. Mabrouk, Y. E. Choonara, P. Kumar, L. C. du Toit, P. P. D. Kondiah and V. Pillay, *Carbohydr. Polym.*, 2017, **157**, 1215–1225.
- 26 J. Grenier, H. Duval, F. Barou, P. Lv, B. David and D. Letourneur, *Acta Biomater.*, 2019, **94**, 195–203.
- 27 F. Dehli, A. Southan, W. Drenckhan and C. Stubenrauch, *J. Colloid Interface Sci.*, 2021, **588**, 326–335.
- 28 B. Göttel, J. M. de Souza, E. Silva, C. Santos De Oliveira, F. Syrowatka, M. Fiorentzis, A. Viestenz, A. Viestenz and K. Mäder, *Eur. J. Pharm. Biopharm.*, 2020, **146**, 125–132.
- 29 K. Ziv, H. Nuhn, Y. Ben-Haim, L. S. Sasportas, P. J. Kempen, T. P. Niedringhaus, M. Hrynyk, R. Sinclair, A. E. Barron and S. S. Gambhir, *Biomaterials*, 2014, **35**, 3736–3743.
- 30 C. Ji, A. Khademhosseini and F. Dehghani, *Biomaterials*, 2011, **32**, 9719–9729.
- 31 T. Asoh, M. Matsusaki, T. Kaneko and M. Akashi, *Adv. Mater.*, 2008, **20**, 2080–2083.
- 32 G. Alamé and L. Brassart, *Soft Matter*, 2019, **15**, 5703–5713.
- 33 K. Kothari, Y. Hu, S. Gupta and A. Elbanna, *J. Appl. Mech.*, 2018, **85**, 031008.
- 34 J. Lei, Z. Li, S. Xu and Z. Liu, *J. Mech. Phys. Solids*, 2021, **156**, 104599.
- 35 J. Lei and Z. Liu, *J. Appl. Phys.*, 2022, **132**, 135101.
- 36 J. F. Marko and E. D. Siggia, *Macromolecules*, 1995, **28**, 8759–8770.
- 37 J. R. Rice, *J. Appl. Mech.*, 1968, **35**, 379–386.
- 38 M. I. Giannotti and G. J. Vancso, *ChemPhysChem*, 2007, **8**, 2290–2307.
- 39 R. S. Rivlin and A. G. Thomas, *J. Polym. Sci.*, 1953, **10**, 291–318.
- 40 K. Guo, B. Ni and H. Gao, *Int. J. Fract.*, 2020, **222**, 13–23.
- 41 E. M. Arruda and M. C. Boyce, *J. Mech. Phys. Solids*, 1993, **41**, 389–412.
- 42 W. Kuhn and F. Grün, *Kolloid-Z.*, 1942, **101**, 248–271.
- 43 L. R. G. Treloar, *Trans. Faraday Soc.*, 1954, **50**, 881.
- 44 J. S. Palmer and M. C. Boyce, *Acta Biomater.*, 2008, **4**, 597–612.
- 45 E. E. Gdoutos, *Fracture mechanics: An introduction*, Springer International Publishing, Cham, 2020, vol. 263.
- 46 B. Chen, X. Shi and H. Gao, *Proc. R. Soc. London, Ser. A*, 2008, **464**, 657–671.
- 47 C. Li, H. Yang, Z. Suo and J. Tang, *J. Mech. Phys. Solids*, 2020, **134**, 103751.
- 48 B. Deng, S. Wang, C. Hartquist and X. Zhao, *Phys. Rev. Lett.*, 2023, **131**, 228102.
- 49 C. Hartquist, S. Wang, Q. Cui, W. Matusik, B. Deng and X. Zhao, *arXiv*, 2024, preprint, arXiv:arXiv:2401.05564, <https://arxiv.org/abs/2401.05564>.
- 50 S. Wang, H. K. Beech, B. H. Bowser, T. B. Kouznetsova, B. D. Olsen, M. Rubinstein and S. L. Craig, *J. Am. Chem. Soc.*, 2021, **143**, 3714–3718.
- 51 H. J. Gao and S. H. Chen, *J. Appl. Mech.*, 2005, **72**, 732–737.
- 52 M. Hua, S. Wu, Y. Ma, Y. Zhao, Z. Chen, I. Frenkel, J. Strzalka, H. Zhou, X. Zhu and X. He, *Nature*, 2021, **590**, 594–599.
- 53 T. Yang, Z. Jia, Z. Wu, H. Chen, Z. Deng, L. Chen, Y. Zhu and L. Li, *Nat. Commun.*, 2022, **13**, 1–12.
- 54 A. Ural and D. Vashishth, *Int. Mater. Rev.*, 2014, **59**, 245–263.

